Photoluminescence of excitons bound to the isoelectronic hydrogen-related defects B_{80}(1.1470 eV) and B^{1}_{19}(1.1431 eV) in silicon

A. S. Kaminskii and E. V. Lavrov
Institute of Radioengineering and Electronics, Russian Academy of Sciences, 11 Mohovaya Street, Moscow, 103907, Russia

V. A. Karasyuk and M. L. W. Thewalt
Department of Physics, Simon Fraser University, Burnaby, British Columbia, Canada V5A 1S6

(Received 21 July 1994)

Photoluminescence spectra of excitons bound to isoelectronic defects B_{80} and B^{1}_{19} (1.147 00- and 1.143 14-eV principal no-phonon lines, respectively), created in phosphorous-doped silicon grown in a hydrogen atmosphere as the result of irradiation by thermal neutrons, were investigated in magnetic fields up to 12 T and under uniaxial stress in ⟨001⟩, ⟨111⟩, and ⟨110⟩ crystallographic directions using high-resolution Fourier-transform spectroscopy. The symmetry of these defects was determined to be C_1. The ground state of the bound excitons is split into a triplet. The lowest state, which is not evident in the zero-field spectra, results in an additional spectral component under applied magnetic field. Using group theory, we constructed a Hamiltonian for excitons bound to the isoelectronic centers B_{80} and B^{1}_{19}, which takes into account electron-hole coupling and interactions with external perturbations. g-factors $g^{x}_{1/2}=1.3$, $g^{y}_{1/2}=1.2$, $g^{z}_{1/2}=0.6$, $g^{x}_{3/2}=0.9$, $g^{y}_{3/2}=1.2$, $g^{z}_{3/2}=1.7$ for B_{80} and $g^{x}_{1/2}=1.35$, $g^{y}_{1/2}=1.6$, $g^{z}_{1/2}=0.7$, $g^{x}_{3/2}=0.9$, $g^{y}_{3/2}=0.7$, $g^{z}_{3/2}=1.56$ for B^{1}_{19} were determined from the best fit to the experiment.

I. INTRODUCTION

The effects of hydrogen impurities on the properties of semiconductors have become an object of increasingly intensive studies. In some cases, doping with hydrogen improves considerably the electronic characteristics of the material due to the neutralization of the undesirable influence of residual defects and impurities (hydrogen passivation), or by introducing new defects with desirable properties. These effects have been studied most extensively in germanium, but similar effects in silicon have recently attracted the attention of many researchers.

The investigation of excitons bound to hydrogen-related radiation-damage defects in semiconductors provides valuable information about the types of bonds between hydrogen and other impurity atoms in silicon. The defects B_{80} and B^{1}_{19} are radiation-damage defects, which bind excitons with unusually small localization energies (8.0 and 11.9 meV, respectively). These defects were discovered recently in silicon grown in a hydrogen atmosphere by Kaminskii *et al.*[1,2] who suggested that these isoelectronic centers contain hydrogen. Safonov[3] and Lightowlers, using a comparison between photoluminescence (PL) spectra of hydrogen and deuterium-doped silicon, demonstrated that both defects incorporate at least three hydrogen atoms.

Kaminskii *et al.*[1,2] reported several excited electronic states of bound excitons (BE's) on the isoelectronic centers B_{80} and B^{1}_{19}, which control the lifetime of BE's because electron-hole recombination in the ground state is partially forbidden.[2] The goal of the present work was to study the electronic structure of excitons bound to the centers B_{80} and B^{1}_{19} and to determine the symmetry of these defects by means of high-resolution magneto- and piezo- PL spectroscopy.

II. EXPERIMENTAL TECHNIQUE

The samples were cut from a phosphorus-doped (phosphorus concentration 2×10^{14} cm^{-3}) silicon grown in a hydrogen atmosphere by the floating-zone technique. The samples were irradiated with a beam of thermal neutrons at a dose of 10^{17} cm^{-2}, corresponding to the transmutational phosphorous content of 2×10^{12} cm^{-3} (the cadmium number $K=200$). After irradiation, the samples were annealed for 30 min in air at a fixed temperature set in a small range around 450 °C depending on the sample origin.[1,2]

The same samples were used in the Zeeman effect and uniaxial stress measurements. To achieve highly homogeneous strain, the samples were made in a shape of long-square parallelepipeds with dimensions $2\times2\times20$ mm^3 and pyramids on the ends.[5] This allows quick and precise positioning of the samples in a stress rig by putting the tips of the pyramids in small conical holes stamped in the centers of the brass pistons to which force is applied by the push rod with calibrated weights on the top. The sample geometry ensures high homogeneity of the strain field in the middle part of the sample. Long sides of the samples were x-ray oriented in ⟨001⟩, ⟨111⟩, and ⟨110⟩ crystallographic directions.

Zeeman effect measurements were performed in a 12-T superconducting solenoid (Oxford Instruments) with a 2-in. bore. The long side of the sample was oriented parallel to the magnetic field, and luminescence radiation emitted perpendicular to the field (Voigt configuration) was reflected by a mirror towards the window at the bottom of the cryostat. The angular dependences of the Zeeman spitting were measured on a sample of different geometry, which was mounted on a platform attached to a gear mechanism enabling rotation of the sample in a $(1\bar{1}0)$

crystallographic plane parallel to the magnetic field.

The samples were immersed in a liquid He bath and photoexcited by a 0.3-W cw radiation from a Spectra Physics Ti-sapphire laser tuned to a 0.80-μ wavelength. The luminescence spectra were recorded by a BOMEM DA8 Fourier-transform spectrometer with resolution up to 0.02 cm^{-1}. Physical Optics Corporation Raman holographic edge filters were used to prevent scattered laser radiation from falling onto the detector, a cooled $In_xGa_{1-x}As$ photodiode.

In the alternative experimental setup, the sample was excited by a 1-W cw Argon laser and spectra were recorded using a scanning Fabry-Perot interferometer with a cooled photomultiplier tube as a detector operating in a photon counting mode. The spectra in this case were numerically processed using the deconvolution program[6,7] in order to improve spectral resolution.

A pulsed radiation from a semiconductor laser with 1.5-W power in 100-ns pulses was used for the lifetime measurements. Details of these measurements have been described in Ref. 2.

III. RESULTS AND DISCUSSION

The samples of silicon prepared as described in the previous section produced very strong luminescence at liquid He temperatures with the two major spectral features X_{80} and X^1_{19} (Fig. 1) surrounded by several weaker spectral components. Due to a higher spectral resolution, the number of components in our spectra is greater than in Refs. 1 and 2. Within each group, the relative amplitudes of the peaks depend on the temperature in a way consistent with thermal population of the energy levels corresponding to peak positions. On the other hand, the amplitude ratio of the components X_{80} and X^1_{19} depends on the annealing temperatures of the sample but not on the temperatures at which the spectra were recorded, suggesting that these lines correspond to different centers. This is the case also for one of the weaker components labeled as X^1_{18}. This component is dominant in the spectra of vacuum-grown silicon doped with germanium in concentration $5\times10^{16}-1\times10^{17}$ cm^{-3} after irradiation by thermal neutrons and 30-min. anneal at 450 °C (Fig. 2). Therefore, we believe that the component X^1_{18} is due to yet another center, which will be referred to as B^1_{18}. The spectrum in Fig. 2 was recorded using a scanning Fabry-Perot interferometer and was numerically processed using a deconvolution program.[6] Besides the components from 0 to 3 related to the centers B^1_{18}, it contains a relatively weak component X^1_{19}, which indicates the presence of significant amount of hydrogen in the sample, although it was not introduced intentionally. The inset in Fig. 2 illustrates the results of lifetime measurements for excitons bound to the centers B^1_{18} at two temperatures. At 4.2 K, the lifetime is 50 μs and at 2 K it is 86 μs, which is very close to the lifetime of excitons bound to the centers B^1_{19}, 45 and 69 μs, respectively.[2] This was the reason why the line X^1_{18} was ascribed previously[2] to the defect B^1_{19}.

The inset in Fig. 1 shows a proposed energy-level diagram for the bound excitons in question, which is qualita-

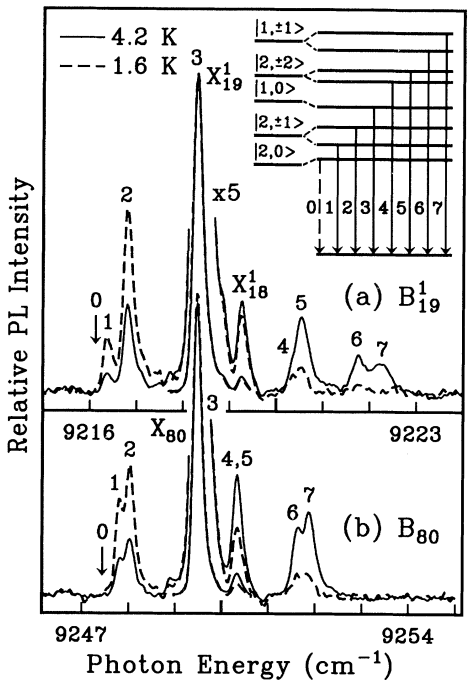

FIG. 1. PL spectra of excitons bound to the centers B^1_{19} (a) and B_{80} (b) taken at 4.2 K (solid lines) and 1.6 K (dashed lines). The spectra are normalized to match the amplitudes of the PL peaks X_{80} and X^1_{19}. The numbers from 0 to 7 label the PL peaks corresponding to the optical transitions shown in the inset. Classification of the BE states is given in Sec. III and in the Appendix. Arrows in the spectra and the dashed arrowed line in the inset indicate the transition 0, which is not observable in the absence of external perturbations.

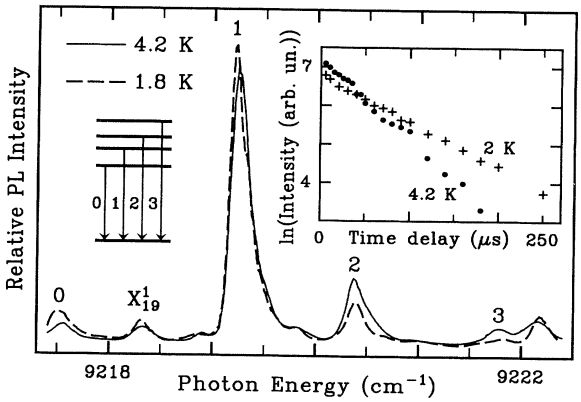

FIG. 2. PL spectra of excitons bound to the centers B^1_{18}. The spectra are normalized to match the amplitudes of the PL peaks X^1_{18} at 4.2 (solid lines) and 1.8 K (dashed lines). The numbers from 0 to 3 label the PL peaks corresponding to the optical transitions shown in the inset. The inset shows the logarithm of the X^1_{18} intensity as a function of delay between the excitation and the 5-μs probe pulses in the BE lifetime measurements at 4.2 and 2 K.

tively the same for the centers B_{80} and B^1_{19}. These bound excitons contain an electron in one of the two spin $\frac{1}{2}$ states $\alpha=|\frac{1}{2};+\frac{1}{2}\rangle$, $\beta=|\frac{1}{2};-\frac{1}{2}\rangle$ and a hole in a state, which can be described by the canonical basis of four functions $|j;m_j\rangle$ where $j=\frac{3}{2}$ is the angular momentum and $m_j=\pm\frac{3}{2}$, $\pm\frac{1}{2}$ is the projection of the angular momentum along some arbitrary axis. We will describe the bound-exciton wave functions in two bases, the basis of the products of the canonical single-particle functions:

$$|\tfrac{3}{2};+\tfrac{3}{2}\rangle\alpha,\ |\tfrac{3}{2};+\tfrac{3}{2}\rangle\beta,\ |\tfrac{3}{2};+\tfrac{1}{2}\rangle\alpha,\ |\tfrac{3}{2};+\tfrac{1}{2}\rangle\beta\ ,$$
$$|\tfrac{3}{2};-\tfrac{3}{2}\rangle\alpha,\ |\tfrac{3}{2};-\tfrac{3}{2}\rangle\beta,\ |\tfrac{3}{2};-\tfrac{1}{2}\rangle\alpha,\ |\tfrac{3}{2};-\tfrac{1}{2}\rangle\beta\ , \quad (1)$$

and the basis of functions $|J,M_J\rangle$ with total angular momentum J and its projection M_J:

$$|2;0\rangle,\ |2;\pm1\rangle,\ |1;0\rangle,\ |2;\pm2\rangle,\ |1;\pm1\rangle\ . \quad (2)$$

The detailed forms of the bases (1) and (2) are described in the Appendix. The basis (1) is more convenient for the construction of the Hamiltonian and the basis (2) is more convenient for the calculation of the optical-transition probabilities. Relations between the matrices of operators in the bases (1) and (2) are also given in the Appendix. In our model, the centers B_{80} and B^1_{19} possess the lowest possible symmetry described by the point group C_1 because experimental results cannot be accounted for even qualitatively in a model with higher symmetry. The point group C_1 has only one-dimensional representations; therefore, the Hamiltonian in the bases (1) or (2) with such symmetry produce eight different energy levels if there is no accidental degeneracy. These energy levels and corresponding optical transitions are labeled with the numbers from 0 to 7 in Fig. 1. One can see in the spectra in Fig. 1 only seven spectral components related to the centers B^1_{19} and six components related to the centers B_{80}. However, the component 0 emerges in the spectra with rapidly growing intensity in magnetic fields (Fig. 3). We assume that the optical recombination in the state 0 is prohibited at zero field, but is allowed when the field is applied. Details of the spectra in magnetic field indicate the presence of both components four and five, which merge together at zero field, so the total number of components observed in the spectra is consistent with our model.

In order to provide a quantitative analysis of the results, one needs the explicit form of the BE Hamiltonian. In the previous paper[4] regarding the defects B^{17}_1 we have constructed the Hamiltonian of BE using the method of invariants of Bir and Pikus.[8] This method allows the construction of the exact Hamiltonian; but, in the case of the centers with low symmetry, it results in a very large number of adjustable parameters. Therefore, in this paper, we use a procedure suggested by Gil *et al.*,[9] which enables construction of an approximate Hamiltonian with a considerably fewer number of phenomenological constants.

In the absence of any external perturbation, the eight-dimensional matrix of the BE Hamiltonian can be represented by the sum of the direct products:

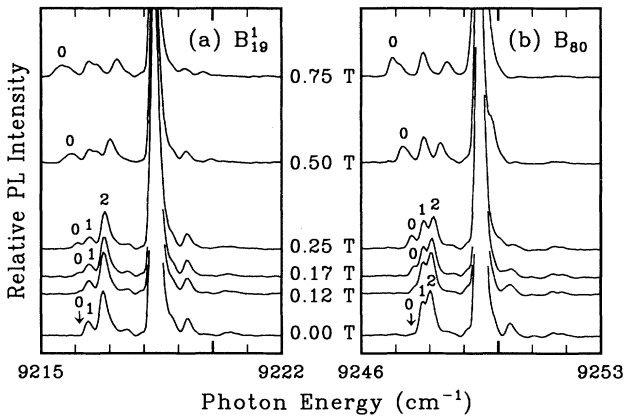

FIG. 3. Evolution of the (a) B^1_{19} and the (b) B_{80} BE PL spectra in weak $\langle 001\rangle$ magnetic fields at 1.8 K recorded in Voigt configuration ($\mathbf{k}\perp\mathbf{B}$) at 0, 0.12, 0.17, 0.25, 0.50, and 0.75 T. The numeric labels correspond to the scheme of transitions shown in Fig. 1. The arrow at 0 T shows the likely position of the peak 0.

$$H_0=\sum_i V_{ii}(J_i^2\otimes\sigma_0)+\frac{\gamma}{4}\sum_i(J_i\otimes\sigma_i),\quad i=x,y,z\ , \quad (3)$$

where J_i are the four-dimensional matrices of the $\frac{3}{2}$ angular-momentum operator written in the canonical basis, σ_i are the Pauli matrices, σ_0 is a two-dimensional unit matrix, γ is a constant of the electron-hole exchange, and V_{ii} represents the diagonal matrix elements of the defect potential calculated on the p-like functions transforming as X, Y, and Z. It is more convenient to use parameters $\delta_1=-\frac{1}{2}V_{zz}$ and $\delta_2=\frac{1}{2}(V_{yy}-V_{xx})$ instead of V_{ii}. The first term in Eq. (3) represents the interaction of the hole with the defect potential and the second term describes the electron-hole exchange in the spherical approximation. The explicit form of the Hamiltonian matrix (3) in the basis of functions (2) is shown in the Appendix [Eq. (A3)–(A5)]. This matrix can be obtained from the matrix (3) of Hamiltonian H_0 in the basis (1) using the equivalence transformation $U^{-1}H_0U$ with the explicit form of the transformation matrix U shown in the Appendix. The matrix H_0 in the basis (2) can be divided into blocks 4×4 with off-diagonal blocks equal to zero, which makes interpretation of the results much easier. In this approximation, only those states are optically active that contain in their expansion in the basis (2) the functions $|1;0\rangle$ and/or $|1;\pm1\rangle$. The matrix H_{11} [Eq. (A4)] has a zero element on the intersection of the row $|2;0\rangle$ and the column $|1;0\rangle$, therefore, in our approximation, the state $|2;0\rangle$ does not have an admixture of the optically active state $|1;0\rangle$. As a consequence, the transition 0 associated with the state $|2;0\rangle$ can be observed in the spectra only when an external perturbation such as a magnetic field admixes optically active states with the state $|2;0\rangle$. In general, admixture of the optically active states to the optically inactive states is small, which is indicated by the smallness of the splittings in the zero-field spectra as compared to BE localization energy. Therefore, the spectral components in Fig. 1 corresponding to

the optically inactive states of BE have relatively small amplitudes.

Diagonalization of (3) or (A3) gives the BE energy levels and the corresponding wave functions. The parameters δ_1, δ_2, and γ have been determined unambiguously from the experimental positions of the zero-field spectral components. They are $\delta_1=0.17$, $\delta_2=0.045$, and $\gamma=0.22$ meV for the centers B_{80} and $\delta_1=0.23$, $\delta_2=0.19$, and $\gamma=0.29$ meV for the centers B^1_{19}. Defects with C_1 symmetry can have 24 equivalent orientations in the crystal and we have taken this into account in our calculations. This is especially important in the calculations of the spectra in magnetic fields when orientational splittings can be observed.

To test our model, we have performed spectroscopic measurements in Voigt configurations on excitons bound to the B_{80} and B^1_{19} centers in magnetic fields with $\langle 100\rangle$, $\langle 111\rangle$, and $\langle 110\rangle$ orientations. We also have measured the dependences of the orientational splitting of the ground-state components on the direction of magnetic field at $B=6$ and $B=12$ T. In these measurements, the sample was rotated around its $\langle 110\rangle$ crystallographic axis, which was perpendicular to the magnetic field. Some of the results of our measurements in magnetic fields are illustrated in Figs. 4 and 5.

Qualitative analysis shows consistency of the Zeeman effect data with the energy-level diagram presented in Fig. 1. For instance, the narrow spectral component labeled as 4,5 in Fig. 1(b) and corresponding to the states $|2;\pm 2\rangle$ splits in magnetic field (Fig. 4) in the same way as do the components 4 and 5 of Fig. 1(a), the rate of splitting being roughly twice that of the components corresponding to the states $|2;\pm 1\rangle$. The states of the BE mix strongly with each other in magnetic fields and the energy levels shift nonlinearly.

For a quantitative analysis of the Zeeman effect, the matrix

$$H(B)=\sum_i [g^i_{1/2}(\mathbf{J}^{1/2}_i\otimes\sigma_0)+g^i_{3/2}(\mathbf{J}^{3/2}_i\otimes\sigma_0) +\tfrac{1}{2}g_e(\mathbf{I}_4\otimes\sigma_i)]B_i,\quad i=x,y,z\ , \tag{4}$$

describing the interaction with magnetic field was added to the H_0 Hamiltonian matrix (3). Here $g^i_{1/2}$, $g^i_{3/2}$, and g_e are the g factors of the hole and the electron; $\mathbf{J}^{1/2}_i$, $\mathbf{J}^{3/2}_i$, and $\mathbf{I}_4$ are the matrices defined by Eq. (A6) in the Appendix. By diagonalizing the sum $H_0+H(B)$ we have determined the BE energy levels depending on the magnetic-field intensity and orientation. By applying all the symmetry transformations of the point group T_d to the system of reference, we have taken into account different equivalent orientations of the defect. In doing so, we have assumed that the system of reference aligned with the defect in which the tensor of g factors is diagonal, forms the Euler angles α, β, and γ with the cubic axes of the crystal. From the optimal fit to the experimental data, we have obtained the following values of these Euler angles and the g factors: $g^x_{1/2}=1.3$, $g^y_{1/2}=1.2$, $g^z_{3/2}=0.6$, $g^x_{3/2}=0.9$, $g^y_{3/2}=1.2$, $g^z_{3/2}=1.7$, and $g_e=2$ with the Euler angles $\alpha=45°$,

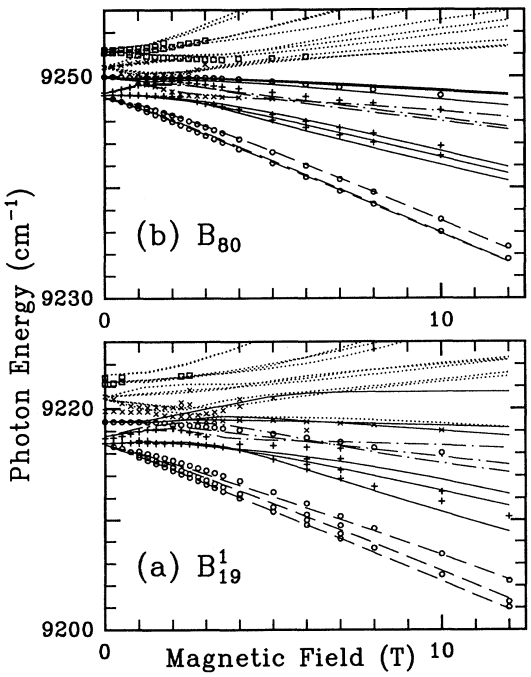

FIG. 4. Dependences of the PL peak positions on the $\langle 001\rangle$ magnetic-field intensity for the BE's on B_{80} and B^1_{19}. Circles, crosses, and squares—experiment; curved lines—theory.

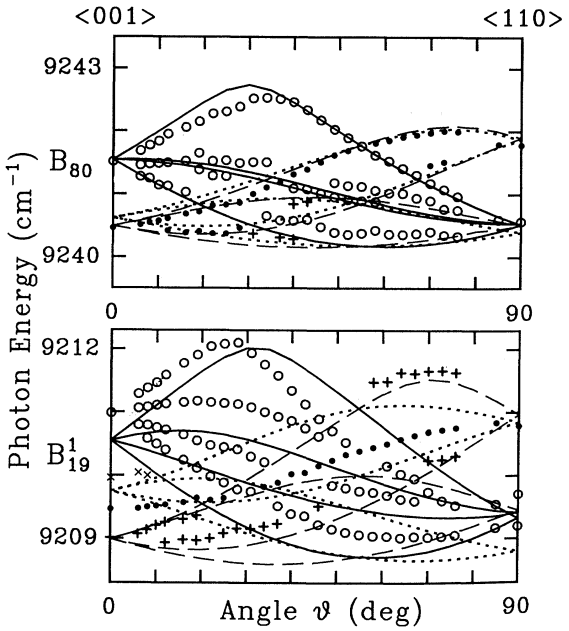

FIG. 5. The ground-state splitting for the BE's on the centers B_{80} (top) and B^1_{19} (bottom) as measured from the PL spectra in magnetic fields with different orientations at 6 T. Circles, crosses, and squares—experiment; curved lines—theory. θ is the angle between magnetic field and the $\langle 001\rangle$ direction in the $(1\bar{1}0)$ crystallographic plane. The splitting is due to the different possible orientations of the defects B_{80} and B^1_{19} with respect to the magnetic field.

$\beta=30°$, and $\gamma=85°$ for the centers B_{80} and $g^x_{1/2}=1.3$, $g^y_{1/2}=1.6$, $g^z_{1/2}=0.7$, $g^x_{3/2}=0.9$, $g^y_{3/2}=0.7$, $g^z_{3/2}=1.56$, and $g_e=2$ with the Euler angles $\alpha=45°$, $\beta=32°$, and $\gamma=85°$ for the centers B^1_{19}. The solid lines in Figs. 4 and 5 show the results of our calculations and dots represent the experimental data. One can see that the proposed model based on the assumption of the C_1 symmetry for the defect provides a good fit to our experimental observations. Figure 4 shows the results for the ⟨001⟩ sample orientation. Similar agreement has been reached for the ⟨111⟩ and ⟨110⟩ orientations. The number of subcomponents evolving in magnetic field from the zero-field ground state is also consistent with the C_1 symmetry of the centers B_{80} and B^1_{19}. For example, in Fig. 5, which shows the positions of the PL peaks as functions of magnetic-field orientation at $B=6$ T, the B_{80} BE ground state splits onto two subcomponents for the ⟨001⟩, three for the ⟨111⟩ and two for the ⟨110⟩ orientation. Similarly, the number of subcomponents of the B^1_{19} BE ground state is three for the ⟨001⟩, four for the ⟨111⟩, and three for the ⟨110⟩ orientation. However, as follows from our calculations with the parameters listed above, some of the components are degenerate and it is likely that in the latter case the number of components is actually three for the ⟨001⟩, four for the ⟨111⟩, and six for the ⟨110⟩. According to Kaplyansky,[10] this pattern of orientational splitting can be observed if the defect symmetry is C_1.

In conclusion, let us consider briefly the effects of uniaxial strain on the PL spectra of excitons bound to the centers B_{80} and B^1_{19}. The PL spectra under uniaxial stress are very complicated and we present in Fig. 6 only the PL peak positions as a function of stress in ⟨001⟩, ⟨110⟩, and ⟨111⟩ directions for the subcomponents of the strongest zero-stress component (component three) of the lines X_{80} and X^1_{19}. One can see that the number of X_{80} subcomponents is three for the ⟨001⟩, five for the ⟨110⟩, and four for the ⟨111⟩ stress directions, while X^1_{19} splits onto three subcomponents for the ⟨001⟩ stress, six for the ⟨110⟩, and four for the ⟨111⟩. This kind of splitting is possibe only for centers with C_1 symmetry.[10]

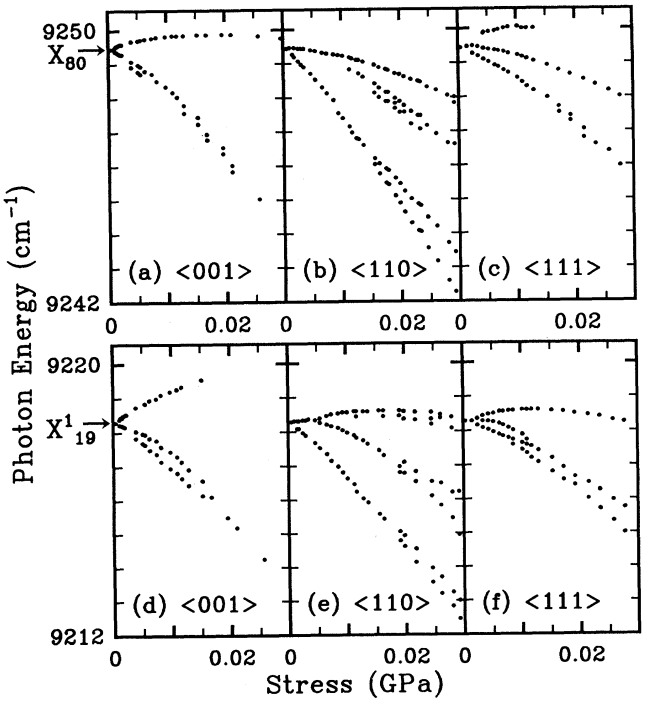

FIG. 6. The PL peak positions (dots) for the subcomponents of the X_{80} and X^1_{19} as a function of uniaxial stress in the ⟨001⟩, ⟨110⟩, and ⟨111⟩ crystallographic directions.

IV. CONCLUSIONS

The results of our photoluminescence spectroscopy for the shallow hydrogen-related radiation-damage isoelectronic centers B_{80} and B^1_{19} in magnetic field and under uniaxial stress show that these centers have the C_1 symmetry. Using the method of Gil *et al.*[9] we have constructed a model Hamiltonian for the excitons bound to these centers, which accounts for the low-symmetry potential of the defect core and for the electron-hole exchange. The interaction parameters in this Hamiltonian have been determined directly from the zero-field spectra. This model Hamiltonian, when combined with the terms describing interaction with magnetic field and uniaxial strain, allows calculation of the BE energy levels in satisfactory agreement with the experiment. The g factors and Euler angles describing orientation of the defects with respect to the cubic crystal aces have been determined from the best fit to the experiment.

ACKNOWLEDGMENTS

The authors wish to thank N. S. Averkiev (Leningrad Physicotechnical Institute, Russian Academy of Science) for the fruitful discussion of the results. This work was supported partly by the Natural Sciences and Engineering Research Council of Canada, by an International Science Foundation long-term research grant, and by an INTAS grant.

APPENDIX

We have used the following two sets of the BE basis functions. The basis (1):

$$|\tfrac{3}{2};+\tfrac{3}{2}\rangle\alpha,\ |\tfrac{3}{2};+\tfrac{3}{2}\rangle\beta,\ |\tfrac{3}{2};+\tfrac{1}{2}\rangle\alpha,\ |\tfrac{3}{2};+\tfrac{1}{2}\rangle\beta\ ,$$
$$|\tfrac{3}{2};-\tfrac{1}{2}\rangle\alpha,\ |\tfrac{3}{2};-\tfrac{1}{2}\rangle\beta,\ |\tfrac{3}{2};-\tfrac{3}{2}\rangle\alpha,\ |\tfrac{3}{2};-\tfrac{3}{2}\rangle\beta\ , \tag{A1}$$

where the hole states are

$$|\tfrac{3}{2};+\tfrac{3}{2}\rangle=\frac{1}{\sqrt{2}}|X+iY\rangle\alpha\ ,$$
$$|\tfrac{3}{2};+\tfrac{1}{2}\rangle=\frac{1}{\sqrt{6}}(|X+iY\rangle\beta-2|Z\rangle\alpha)\ ,$$
$$|\tfrac{3}{2};-\tfrac{1}{2}\rangle=-\frac{1}{\sqrt{6}}(|X-iY\rangle\alpha+2|Z\rangle\beta)\ ,$$
$$|\tfrac{3}{2};-\tfrac{3}{2}\rangle=-\frac{1}{\sqrt{2}}|X-iY\rangle\beta\ ,$$

and the basis (2)

$$
\begin{aligned}
&|2;+2\rangle=|\tfrac{3}{2};+\tfrac{3}{2}\rangle\alpha\ ,\\
&|2;+1\rangle=\tfrac{1}{2}(\sqrt{3}|\tfrac{3}{2};+\tfrac{1}{2}\rangle\alpha+|\tfrac{3}{2};+\tfrac{3}{2}\rangle\beta\ ,\\
&|1;+1\rangle=\tfrac{1}{2}(\sqrt{3}|\tfrac{3}{2};+\tfrac{3}{2}\rangle\beta-|\tfrac{3}{2};+\tfrac{1}{2}\rangle\alpha)\ ,
\end{aligned}
\tag{A2}
$$

$$
\begin{aligned}
&|2;0\rangle=\frac{1}{\sqrt{2}}(|\tfrac{3}{2};-\tfrac{1}{2}\rangle\alpha+|\tfrac{3}{2};+\tfrac{1}{2}\rangle\beta)\ ,\\
&|1;0\rangle=\frac{1}{\sqrt{2}}(|\tfrac{3}{2};+\tfrac{1}{2}\rangle\beta-|\tfrac{3}{2};-\tfrac{1}{2}\rangle\alpha)\ ,\\
&|1;-1\rangle=\tfrac{1}{2}(|\tfrac{3}{2};-\tfrac{1}{2}\rangle\beta-\sqrt{3}|\tfrac{3}{2};-\tfrac{3}{2}\rangle\alpha)\ ,\\
&|2;-1\rangle=\tfrac{1}{2}(|\tfrac{3}{2};-\tfrac{3}{2}\rangle\alpha+\sqrt{3}|\tfrac{3}{2};-\tfrac{1}{2}\rangle\beta)\ ,\\
&|2;-2\rangle=|\tfrac{3}{2};-\tfrac{3}{2}\rangle\beta\ .
\end{aligned}
$$

The relation between the bases (A1) and (A2) can be expressed as (A2) $=\mathbf{U}$ (A1), where $\mathbf{U}$ is a matrix with the following nonzero elements:

$$
\begin{aligned}
&U_{11}=U_{88}=1,\\
&U_{22}=U_{66}=U_{77}=-U_{33}=\tfrac{1}{2}\ ,\\
&U_{23}=U_{32}=U_{76}=-U_{67}=\frac{\sqrt{3}}{2}\ ,\\
&U_{44}=U_{45}=U_{54}=-U_{55}=\frac{1}{\sqrt{2}}\ .
\end{aligned}
$$

In the absence of external perturbations, the Hamiltonian matrix in the basis (A2) has the form

$$
\mathbf{H}_0=\begin{bmatrix}\mathbf{H}_{11} & 0\\ 0 & \mathbf{H}_{22}\end{bmatrix}\ ,
\tag{A3}
$$

with nonzero 4×4 blocks

$$
\mathbf{H}_{11}=\begin{array}{c}
\begin{matrix}|2;+2\rangle & |2;0\rangle & |1;0\rangle & |2;-2\rangle\end{matrix}\\
\left[\begin{matrix}
-\frac{3}{8}\gamma+\delta_1 & \frac{1}{\sqrt{6}}\delta_2 & -\frac{1}{\sqrt{6}}\delta_2 & 0\\
\frac{1}{\sqrt{6}}\delta_2 & -\frac{3}{8}\gamma-\delta_1 & 0 & -\frac{1}{\sqrt{6}}\delta_2\\
-\frac{1}{\sqrt{6}}\delta_2 & 0 & \frac{5}{8}\gamma-\delta_1 & -\frac{1}{\sqrt{6}}\delta_2\\
0 & -\frac{1}{\sqrt{6}}\delta_2 & -\frac{1}{\sqrt{6}}\delta_2 & -\frac{3}{8}\gamma+\delta_1
\end{matrix}\right]
\begin{matrix}|2;+2\rangle\\ |2;0\rangle\\ |1;0\rangle\\ |2;-2\rangle\end{matrix}
\end{array}
\tag{A4}
$$

and

$$
\mathbf{H}_{22}=\begin{array}{c}
\begin{matrix}|2;+1\rangle & |1;+1\rangle & |1;-1\rangle & |2;-1\rangle\end{matrix}\\
\left[\begin{matrix}
-\frac{3}{8}\gamma-\frac{1}{2}\delta_1 & \frac{\sqrt{3}}{2}\delta_1 & -\frac{1}{2\sqrt{3}}\delta_2 & \frac{1}{2}\delta_2\\
\frac{\sqrt{3}}{2}\delta_1 & \frac{5}{8}\gamma+\frac{1}{2}\delta_1 & \frac{1}{2}\delta_2 & \frac{1}{2\sqrt{3}}\delta_2\\
-\frac{1}{2\sqrt{3}}\delta_2 & \frac{1}{2}\delta_2 & \frac{5}{8}\gamma+\frac{1}{2}\delta_1 & -\frac{\sqrt{3}}{2}\delta_1\\
\frac{1}{2}\delta_2 & \frac{1}{2\sqrt{3}}\delta_2 & -\frac{\sqrt{3}}{2}\delta_1 & -\frac{3}{8}\gamma-\frac{1}{2}\delta_1
\end{matrix}\right]
\begin{matrix}|2;+1\rangle\\ |1;+1\rangle\\ |1;-1\rangle\\ |2;-1\rangle\end{matrix}
\end{array}\ ,
$$

where $\delta_1=-\frac{1}{2}V_{zz}$ and $\delta_2=\frac{1}{2}(V_{yy}-V_{xx})$, $V_{xx}=\langle X|\hat{V}|X\rangle$, $V_{yy}=\langle Y|\hat{V}|Y\rangle$, $V_{zz}=\langle Z|\hat{V}|Z\rangle$.

In the Hamiltonian (4) describing interaction with magnetic field, we have used the following matrices:

$$
\begin{aligned}
&\mathbf{J}_x^{1/2}=\tfrac{1}{2}(\sigma_x\otimes\sigma_x+\sigma_y\otimes\sigma_y),\quad \mathbf{J}_x^{3/2}=\sigma_0\otimes\sigma_x\ ,\\
&\mathbf{J}_y^{1/2}=\tfrac{1}{2}(\sigma_y\otimes\sigma_x-\sigma_x\otimes\sigma_y),\quad \mathbf{J}_y^{3/2}=\sigma_0\otimes\sigma_y\ ,\\
&\mathbf{J}_z^{1/2}=\tfrac{1}{2}(\sigma_x\otimes\sigma_0-\sigma_0\otimes\sigma_x),\quad \mathbf{J}_z^{3/2}=\tfrac{1}{2}(\sigma_0\otimes\sigma_z+\sigma_z\otimes\sigma_0)\ ,
\end{aligned}
\tag{A6}
$$

$\mathbf{I}_4=\sigma_0\otimes\sigma_0$—four-dimensional unit matrix .

[1]A. S. Kaminskii, B. M. Leiferov, and A. N. Safonov, Fiz. Tverd. Tela (Leningrad) **29**, 961 (1987) [Sov. Phys. Solid State **29**, 551 (1987)].

[2]A. S. Kaminskii, A. N. Safonov, and E. V. Lavrov, Fiz. Tverd. Tela (Leningrad) **33**, 859 (1991) [Sov. Phys. Solid State **33**, 488 (1991)].

[3]A. N. Safonov and E. C. Lightowlers, Mat. Sci. Forum **143-147**, 903 (1994).

[4]A. S. Kaminskii, E. V. Lavrov, V. A. Karasyuk, and M. L. W. Thewalt, Phys. Rev. B **50**, 7338 (1994).

[5]A. S. Kaminskii, V. A. Karasyuk, and Ya. E. Pokrovskii, Zh. Eksp. Teor. Fiz. **83**, 2237 (1982) [Sov. Phys. JETP **56**, 1295 (1982)].

[6]V. A. Gel'fgat, E. L. Kosarev, and E. R. Podolyak, Prib. Tekh. Eksp. **5**, 86 (1991) [Instrum. Exp. Tech. (USSR) **34**, 1070 (1991)].

[7]A. S. Kaminskii and A. N. Safonov, Pis'ma Zh. Eksp. Teor. Fiz. **55**, 245 (1992) [JETP Lett. **55**, 242 (1992)].

[8]G. L. Bir and G. E. Pikus, *Simmetrya i Deformatsionnye Effecty v Poluprovodnikakh* (Nauka, Moscow, 1972) [Symmetry and Strain-Induced Effects in Semiconductors (Halsted, New York, 1974)].

[9]B. Gil, J. Camassel, P. Merle, and H. Mathieu, Phys. Rev. B **25**, 3987 (1982).

[10]A. A. Kaplyansky, Opt. Spectrosc. **16**, 329 (1964).